Data overview and local velocity models:

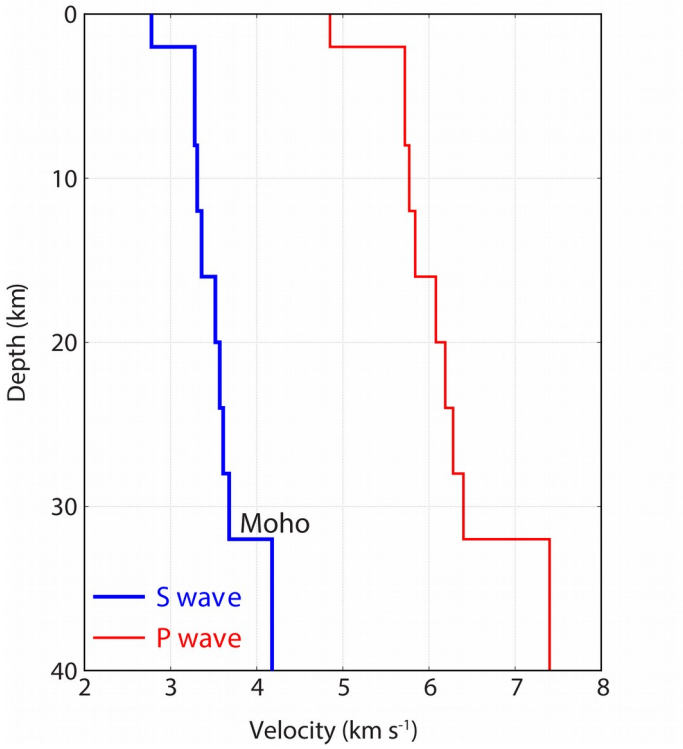

Figure S1. The velocity model for calculating near-field Green's functions.

Figure S2. Distribution of 76 teleseismic broadband stations at distances of 30-80 degrees (red triangles). Focal mechanism of the 24 January 2020 Mw 6.8 Elazığ-Sivrice earthquake. The mechanism coordinate denotes the epicenter.

Wrapped and unwrapped interferograms of the InSAR data:

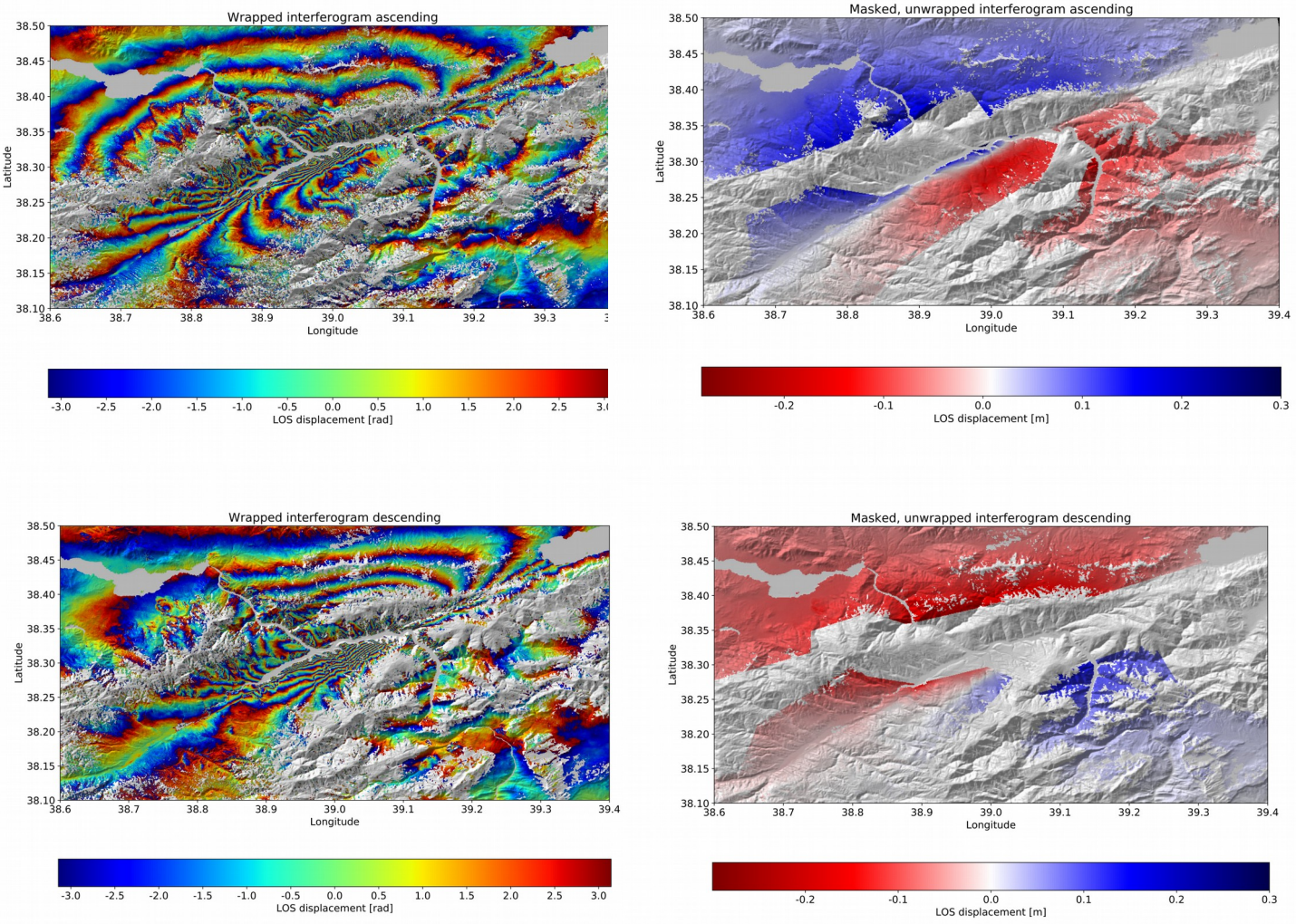

Figure S3. Wrapped (right) and unwrapped (left) interferograms spanning the co-seismic of the Elazığ-Sivrice earthquake for both ascending (up) and descending (down) directions.

Additional evidences for the rupture directivity and regional broadband stations:

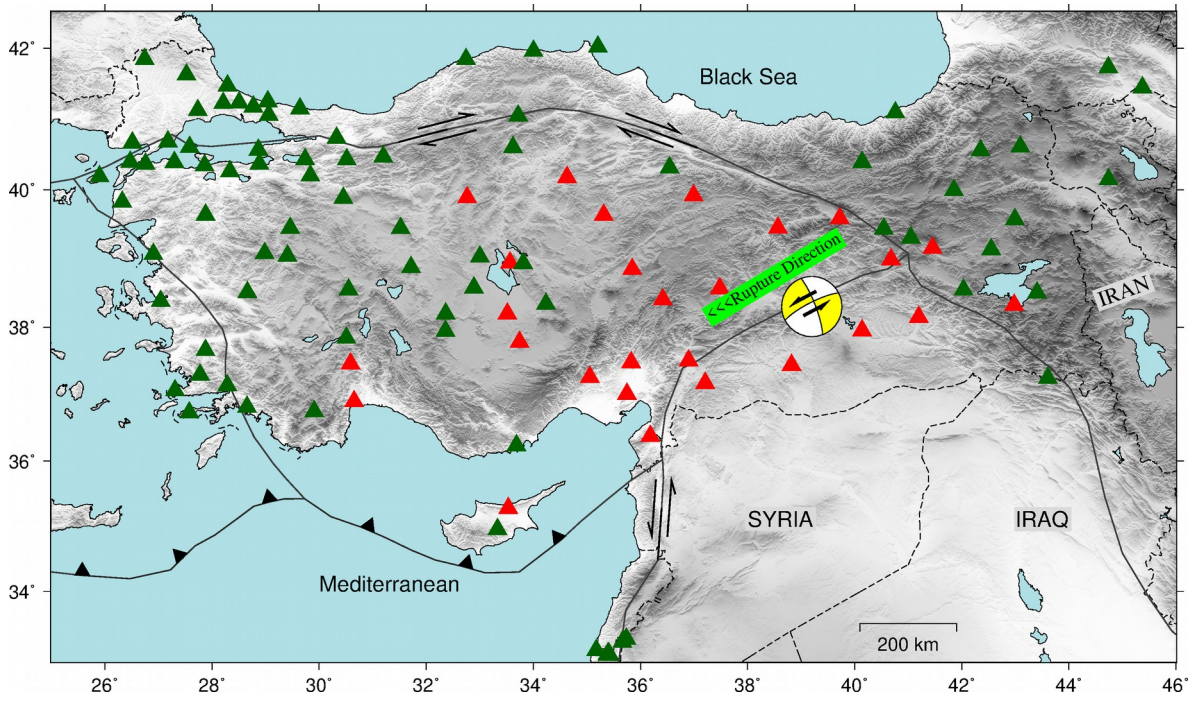

Figure S4. Regional broadband seismic stations of the KOERI and GEOFON networks (triangles) used in this study for the estimation of foreshocks and aftershocks of the Elazığ-Sivrice earthquake, with the observed spatial distribution of saturated seismic stations (red stations). Higher amplitudes have been recorded at stations in the direction of rupture.

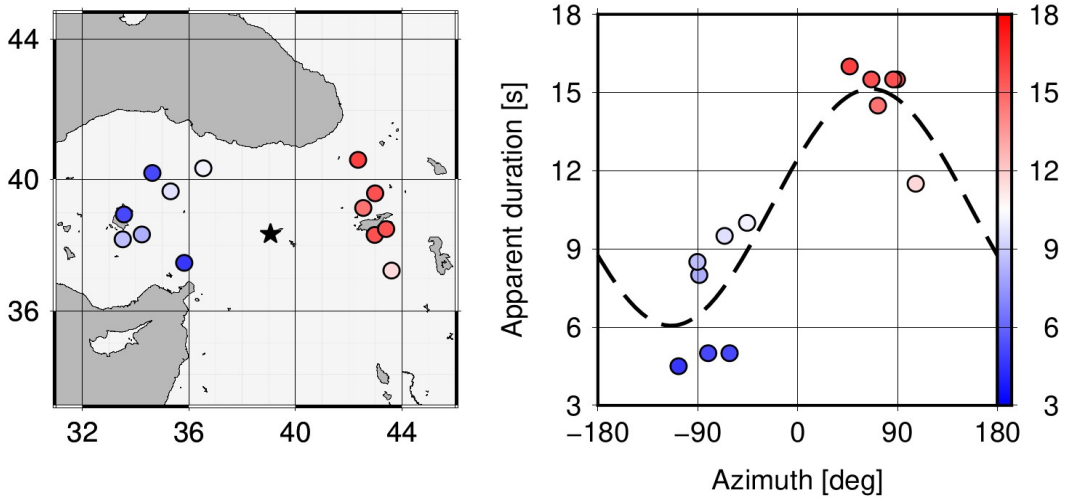

Figure S5. Mainshock apparent rupture duration at regional seismic stations. (left) color-coded in map view and (right) as a function of azimuth. The blue circles which indicate stations in the front of rupture direction, show less apparent duration than those are located in backward of the rupture direction (red circles).

Additional information for the Coulomb failure stress change analysis:

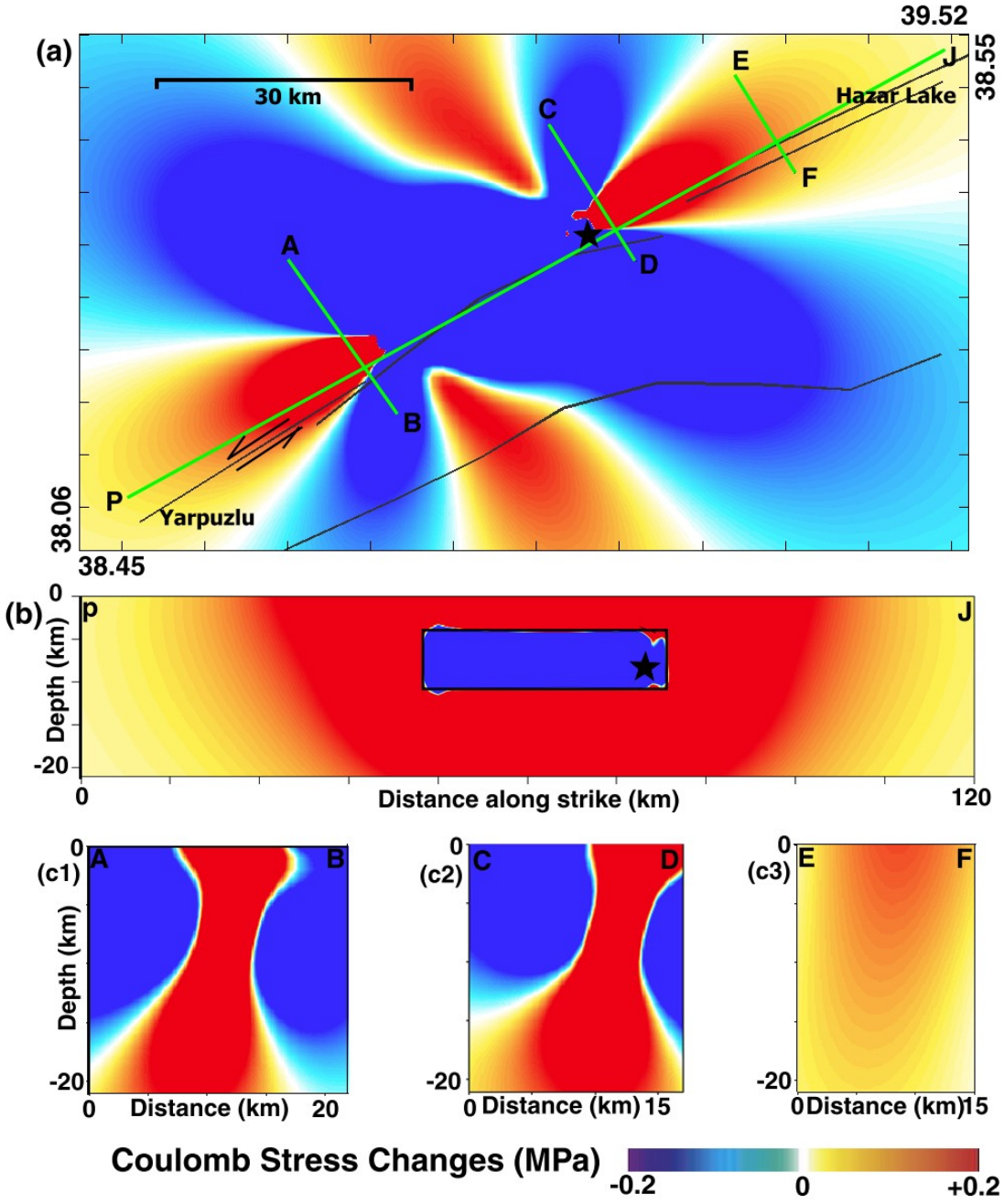

Figure S6. This figure has the same style as Fig. 3.

a) The imparted stress change caused by 24 January 2020 Elazığ-Sivrice earthquake on the surrounding area. Black stars denote the mainshock epicenter and black lines show the main faults in this region (Basili et al., 2013). b) Stress changes on the fault plane along strike (PJ profile). Rectangular shows the main ruptured area. c1, c2, c3) Stress changes on the fault plane along down-dip in 3 different profiles: AB, CD and EF.

Additional information of the moment tensor inversion (mainshock): The figure captions are modified from automated figure generations in the Grond software toolbox (Heimann et al., 2018).

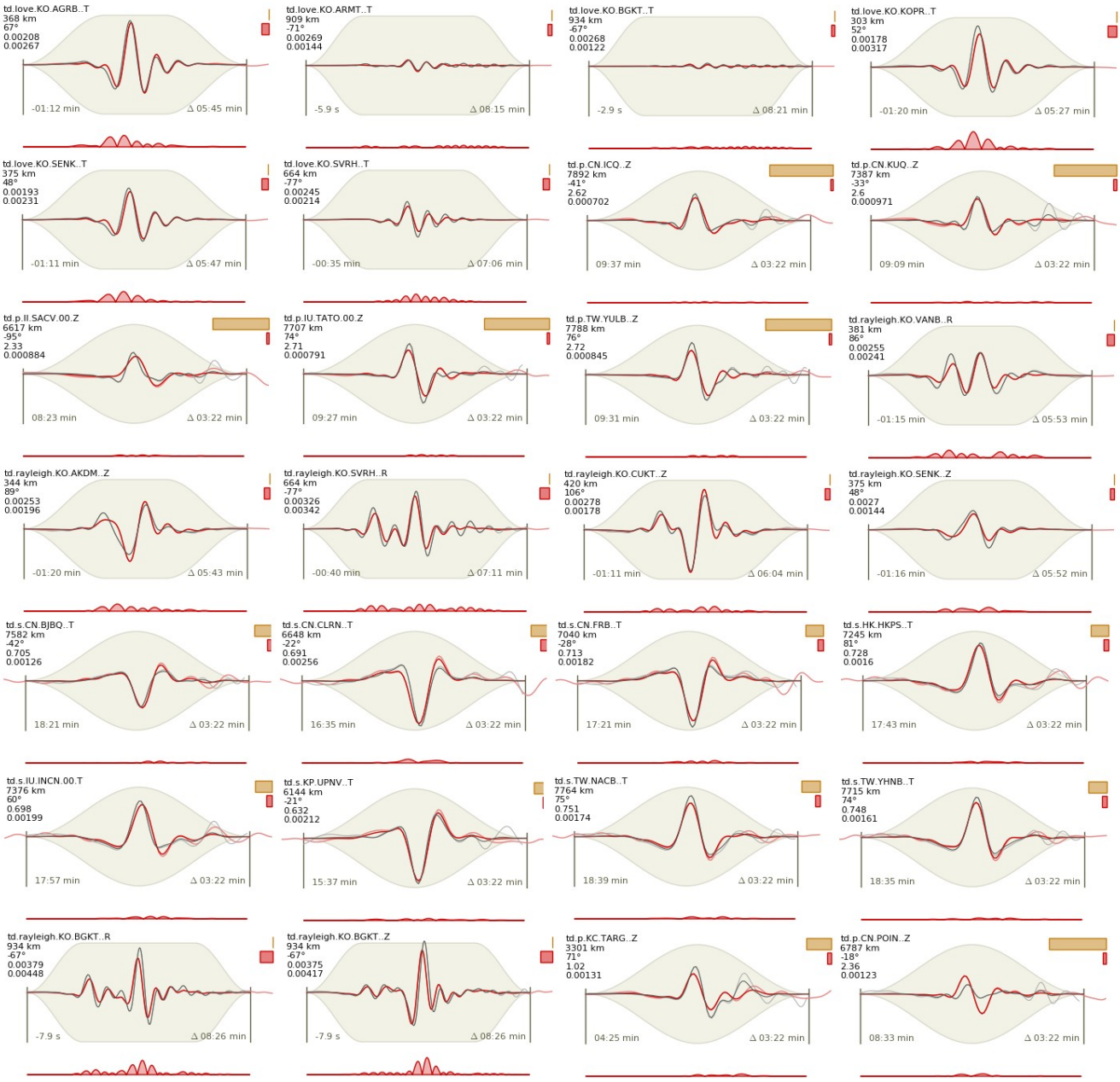

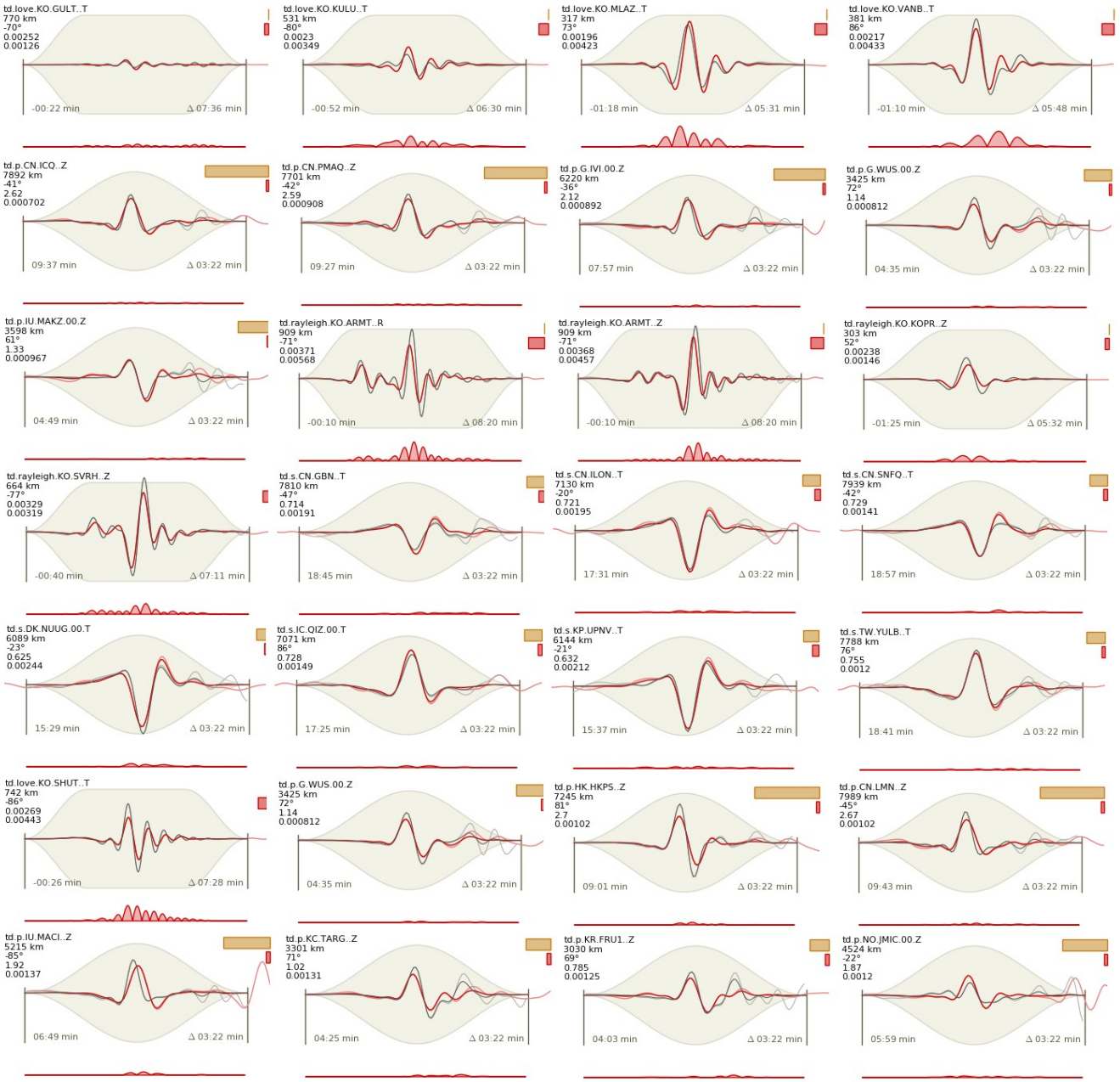

Figure S7. Time domain waveform fits for some selected traces for the best model in teleseimic (P and SH waves: tp.p and td.s) and regional (Rayleigh and Love waves: rd.rayleigh and td.love).

Information (left side, from top to bottom) gives station name with component, distance to source, azimuth of station with respect to source, weight, misfit and starting time of the waveform relative to the origin time. The background gray area shows the applied taper function. The waveforms shown are: the restituted and filtered observed trace (dark gray), the synthetic trace (red). The traces are scaled according to the weight (small weight, small amplitude). Colored boxes on the upper right: Top box (orange) show the relative weight within the entire dataset of the optimization and bottom box (red) the relative misfit contribution to the global misfit of the optimization.

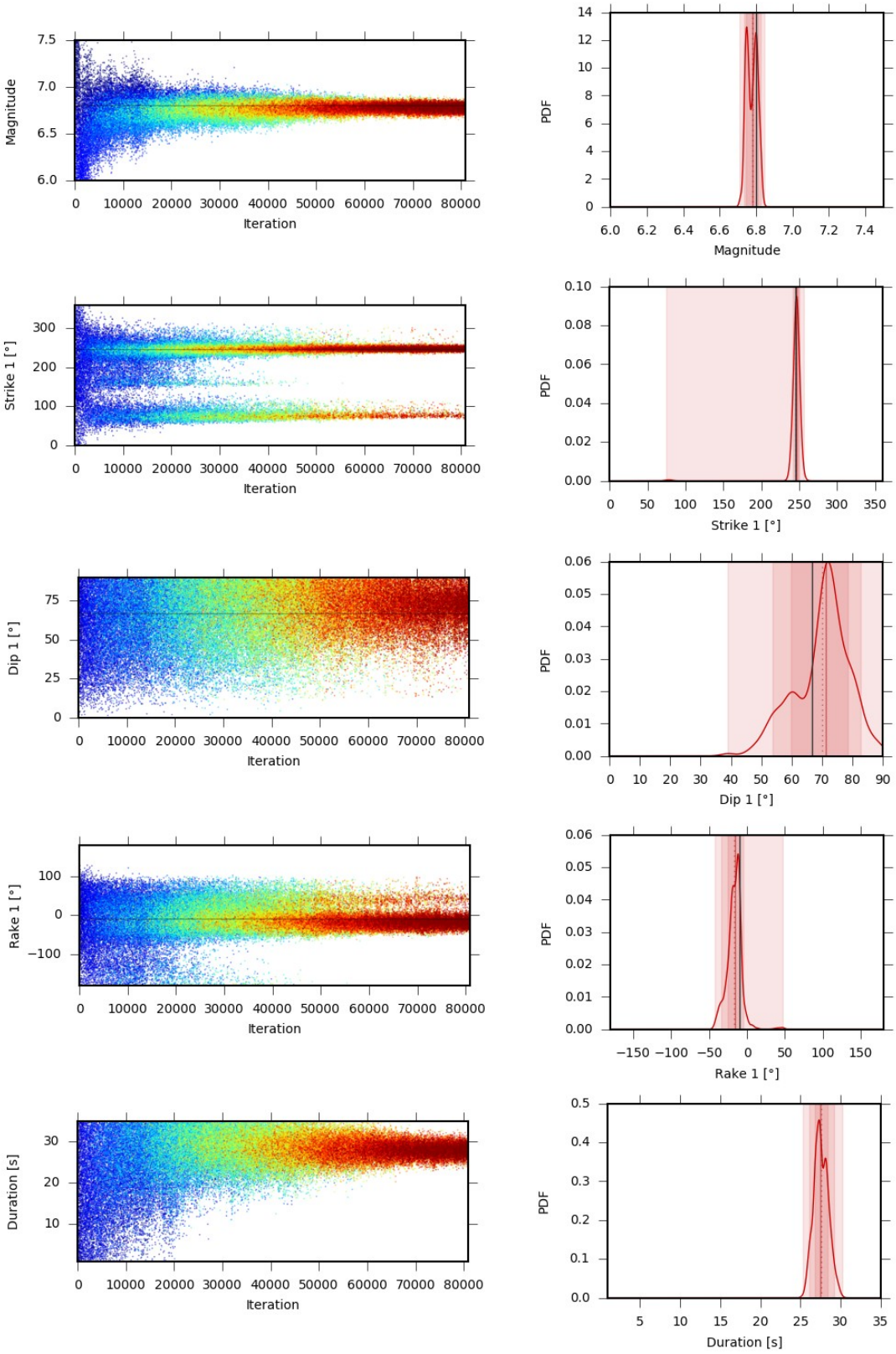
Magnitude
Iteration
PDF
Magnitude
Strike 1 [°]
Iteration
PDF
Strike 1 [°]
Dip 1 [°]
Iteration
PDF
Dip 1 [°]
Rake 1 [°]
Iteration
PDF
Rake 1 [°]
Duration [s]
Iteration
PDF
Duration [s]

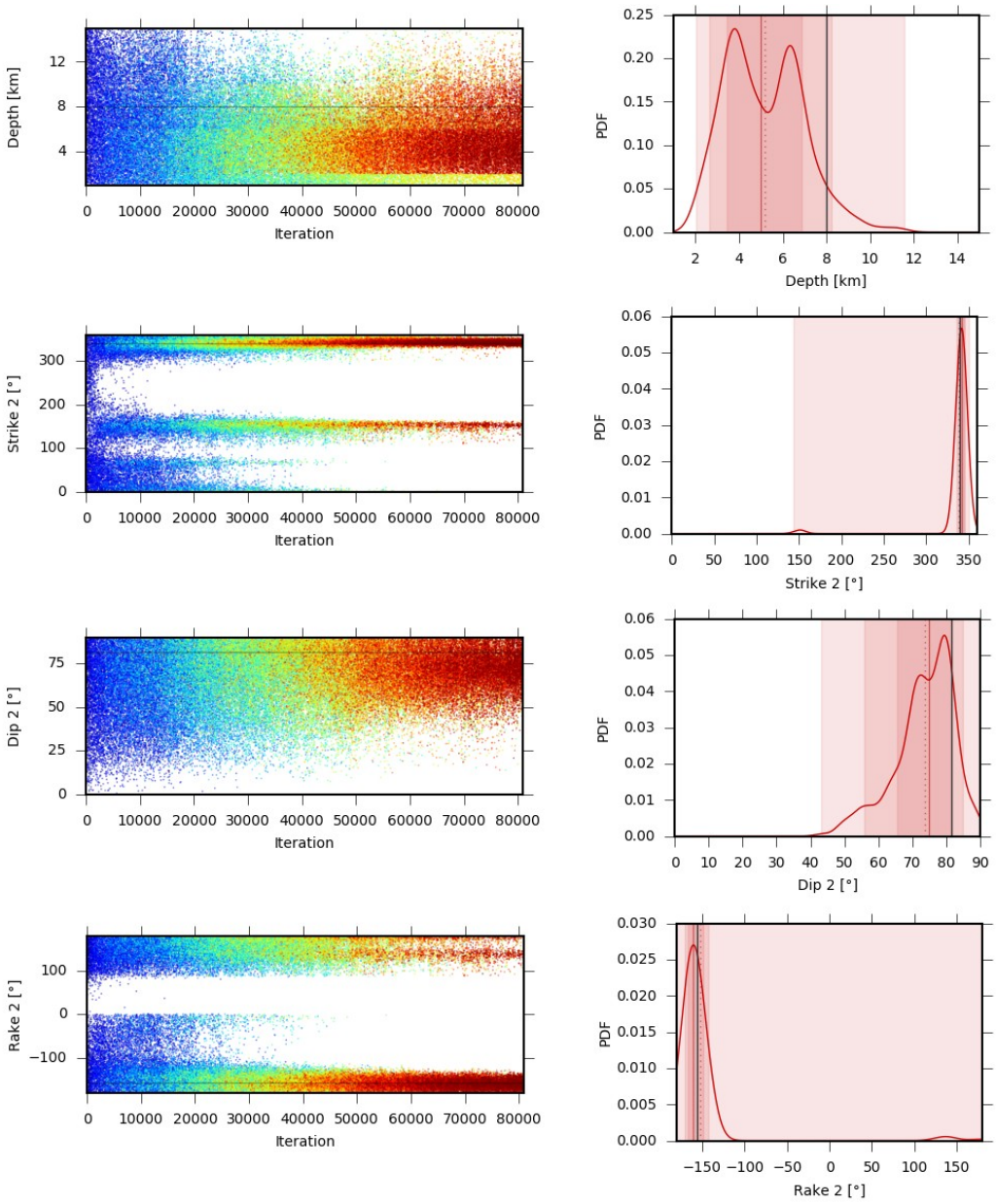

Figure S8. Sequence plot, distribution and uncertainties of the some source parameters (Depth, dips, rakes, strikes, duration and magnitude). Left: The visited parameter values during the optimization is shown. The color shows the relative misfit. Relatively high misfits are in blue colors and relatively low misfits in red. Right: The histograms show Gaussian kernel densities (red curved solid line) of the model parameters (marginals) along with some characteristics: The red solid vertical line gives the median of the distribution and the dashed red vertical line the mean value. Dark gray vertical lines show reference parameter (GCMT solution). The overlapping red-shaded areas show the 68% confidence intervals (innermost area), the 90% confidence intervals (middle area) and the minimum and maximum values (widest area). The plot ranges are defined by the given parameter bounds and show the model space.

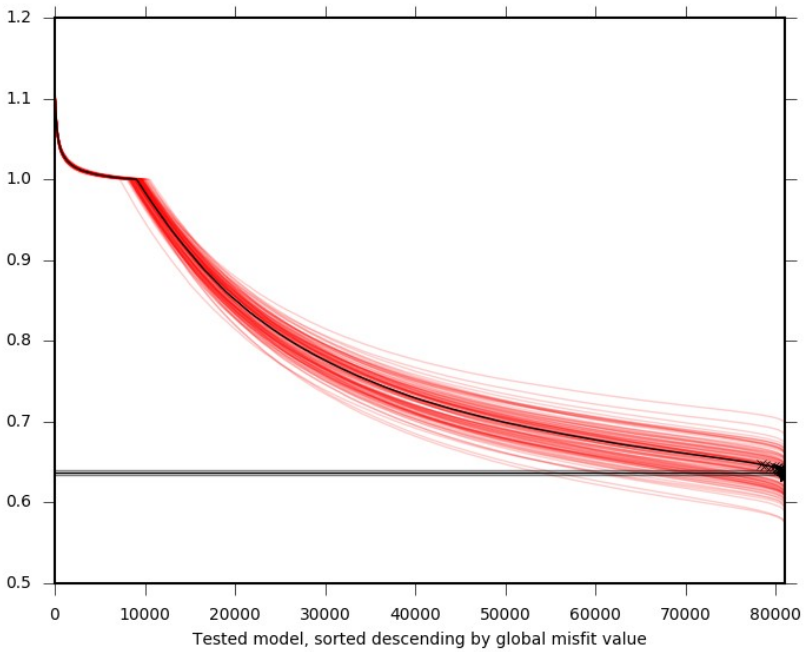

Figure S9. Bootstrap misfit of the optimization in 95000 iterations. For each bootstrap configuration, all models are sorted according to their misfit value (red lines) and their global misfit value (black line). The best model of every bootstrap configuration (right end model of red lines) is marked as a cross in the global misfit configuration.

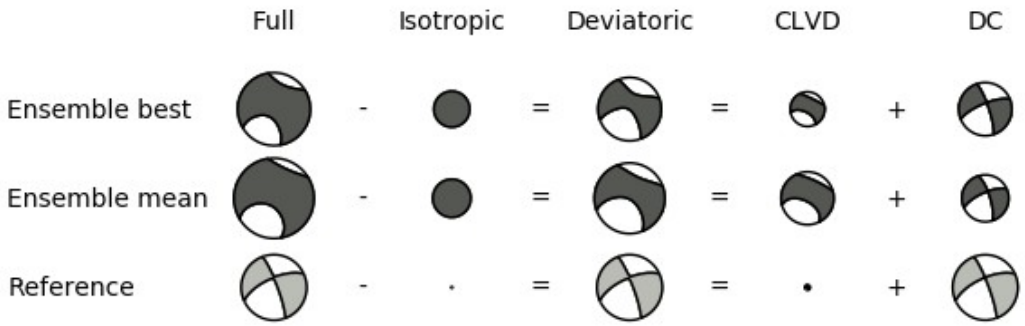

Figure S10. Moment tensor decomposition of the best and mean fitting solution into isotropic, deviatoric and best double couple components. Shown are the ensemble best, the ensemble mean and, a reference mechanism (GCMT). The symbol size indicates the relative strength of the components. Relatively large positive isotropic and negative compensated linear vector dipole (CLVD) components are shown in the moment tensor decomposition. However, to verify and understand the context of the isotropic and CLVD component of the source mechanism requires further investigations, which are beyond the scope of this work.

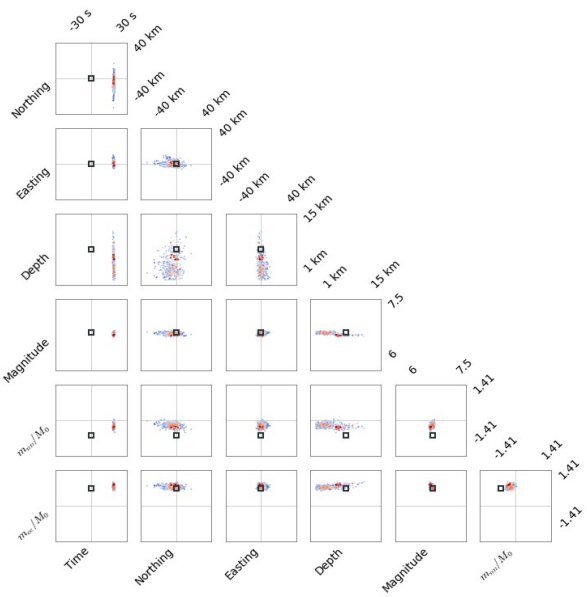
Northing
Easting
Depth
Magnitude
m_{rel}/M_0
m_{rel}/M_0
Time
Northing
Easting
Depth
Magnitude
m_{rel}/M_0

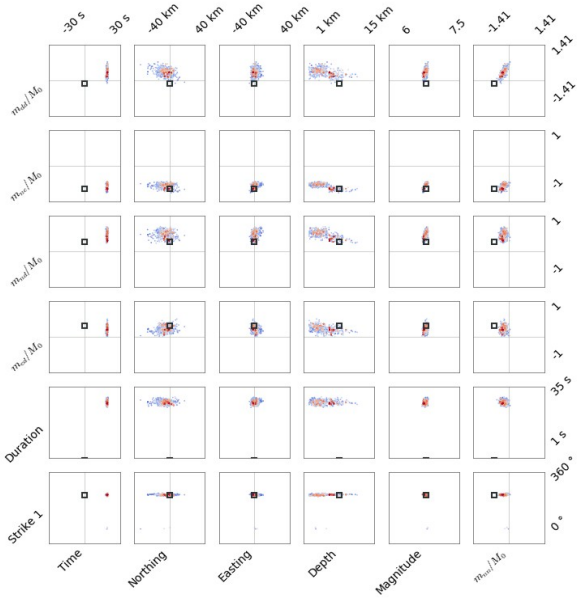
m_{rel}/M_0
m_{rel}/M_0
m_{rel}/M_0
m_{rel}/M_0
Duration
Strike 1
Time
Northing
Easting
Depth
Magnitude
m_{rel}/M_0

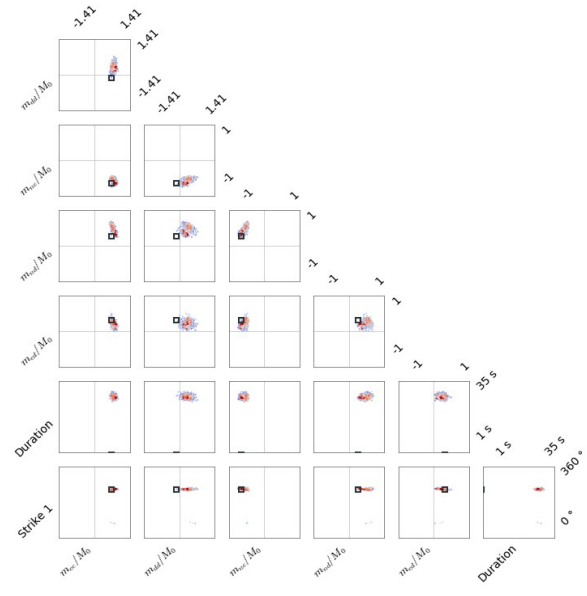
m_{rel}/M_0
m_{rel}/M_0
m_{rel}/M_0
m_{rel}/M_0
Duration
Strike 1
m_{rel}/M_0
m_{rel}/M_0
m_{rel}/M_0
m_{rel}/M_0
m_{rel}/M_0
Duration

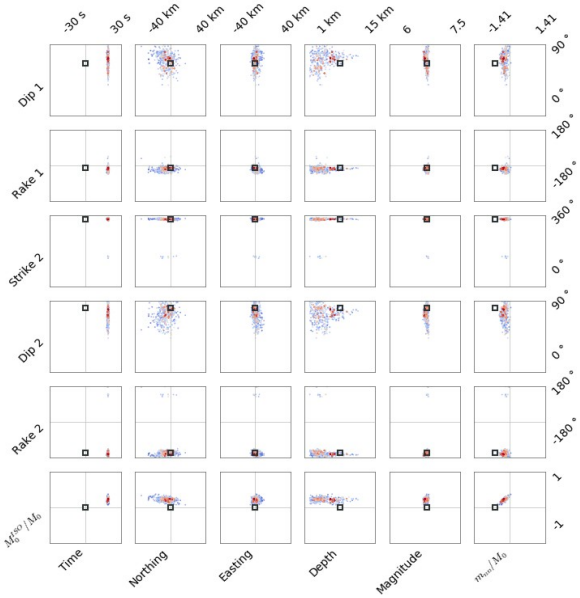
Dip 1
Rake 1
Strike 2
Dip 2
Rake 2
M_0^{iso}/M_0
Time
Northing
Easting
Depth
Magnitude
m_{rel}/M_0

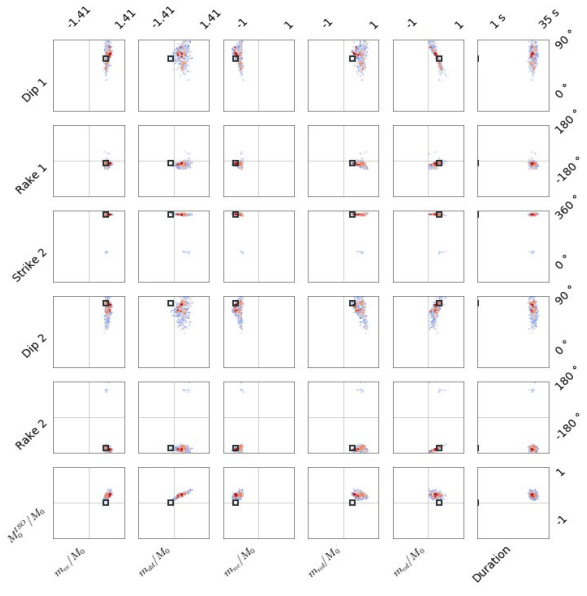
Dip 1
Rake 1
Strike 2
Dip 2
Rake 2
M_0^{iso}/M_0
m_{rel}/M_0
m_{rel}/M_0
m_{rel}/M_0
m_{rel}/M_0
m_{rel}/M_0
Duration

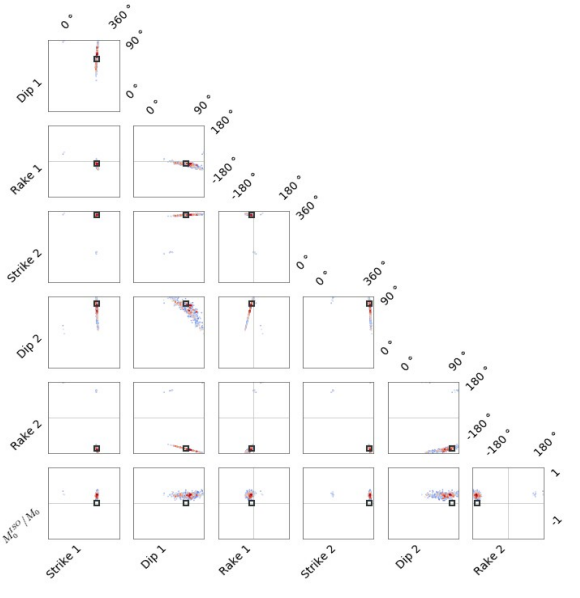
Dip 1
Rake 1
Strike 2
Dip 2
Rake 2
M_0^{iso}/M_0
Strike 1
Dip 1
Rake 1
Strike 2
Dip 2
Rake 2

Figure S11. Source parameter's scatter plots, to evaluate the resolution of source parameters and possible trade-offs between pairs of model parameters. The point color indicates the misfit for the model solution with blue for high misfit models and red for low misfit models. The plot ranges are defined by the given parameter bounds and shows the model space of the optimization. Dark gray boxes mark reference solution (GCMT).

Finite fault model using joint inversion of InSAR and strong motions:

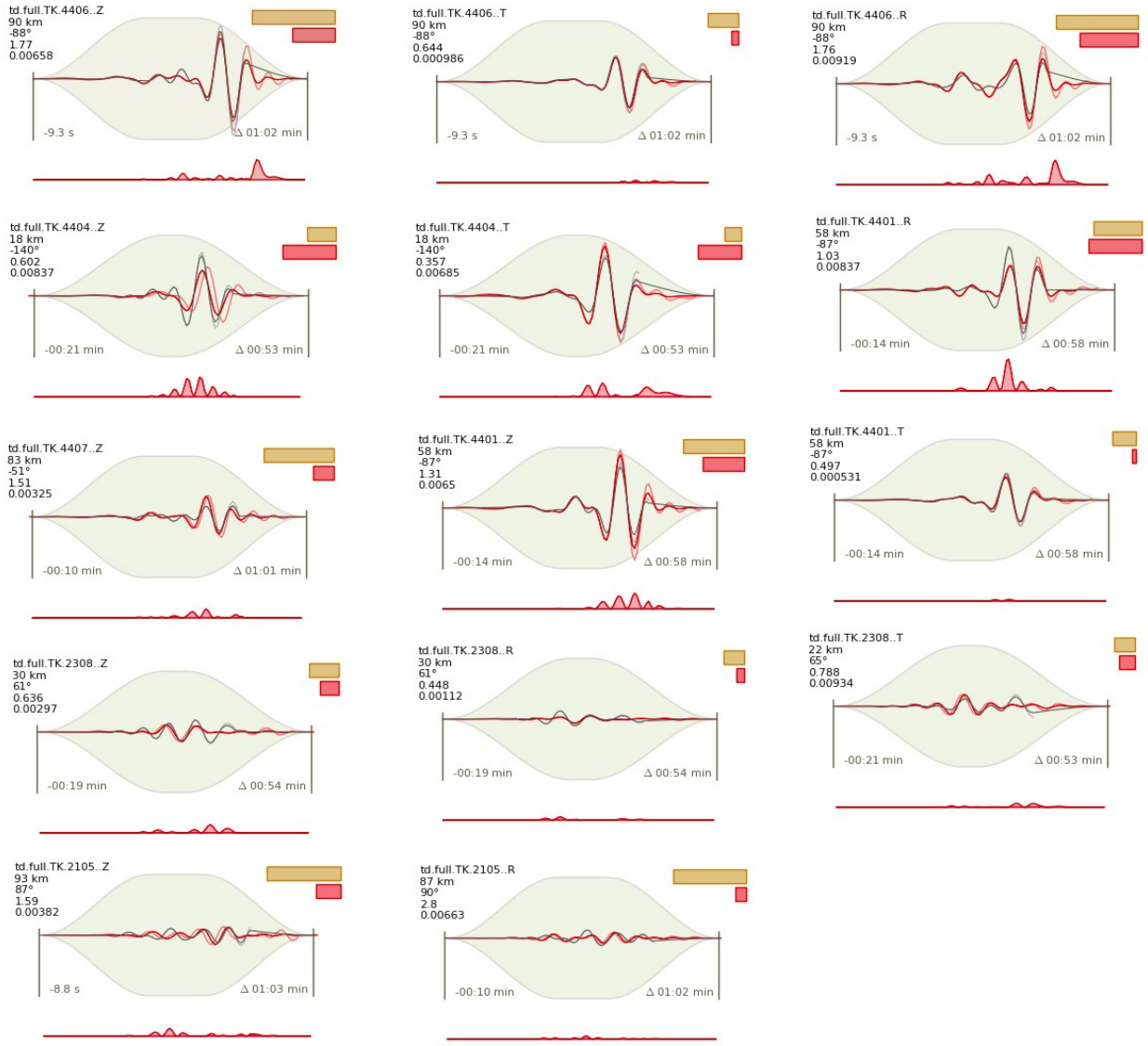

Figure S12. Time domain waveform fits for best model of the strong motion data (full waves: tp.full). For details see caption of Fig. S7.

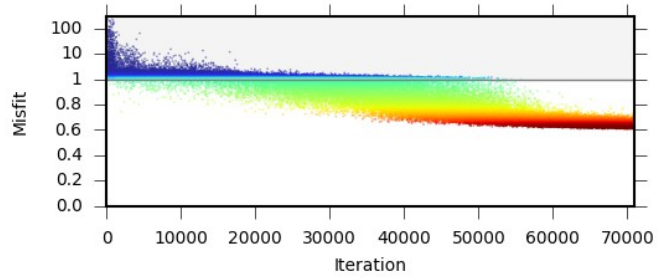
Misfit
100
10
1
0.8
0.6
0.4
0.2
0.0
0
10000
20000
30000
40000
50000
60000
70000
Iteration

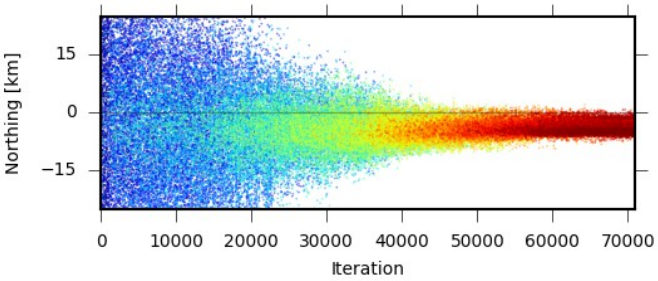
Northing [km]
15
0
−15
0
10000
20000
30000
40000
50000
60000
70000
Iteration

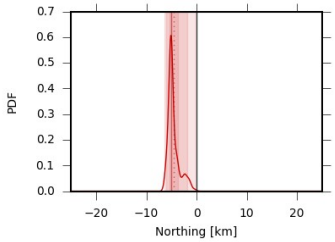
PDF
0.7
0.6
0.5
0.4
0.3
0.2
0.1
0.0
−20
−10
0
10
20
Northing [km]

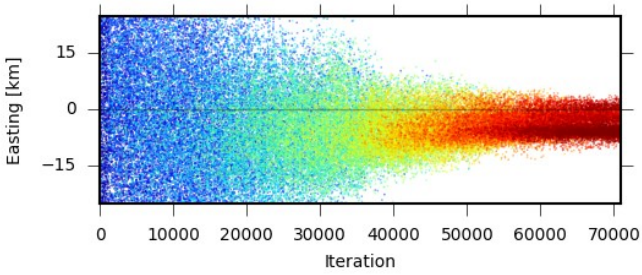
Easting [km]
15
0
−15
0
10000
20000
30000
40000
50000
60000
70000
Iteration

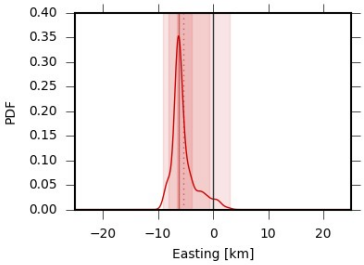
PDF
0.40
0.35
0.30
0.25
0.20
0.15
0.10
0.05
0.00
−20
−10
0
10
20
Easting [km]

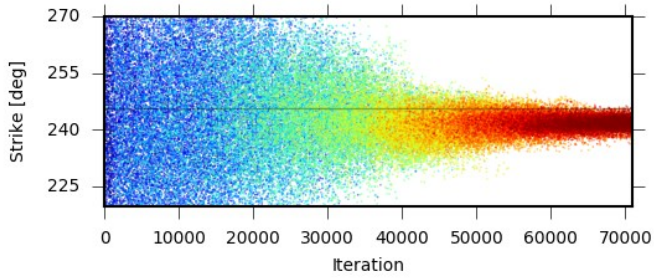
Strike [deg]
270
255
240
225
0
10000
20000
30000
40000
50000
60000
70000
Iteration

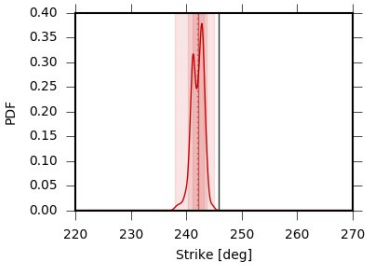
PDF
0.40
0.35
0.30
0.25
0.20
0.15
0.10
0.05
0.00
220
230
240
250
260
270
Strike [deg]

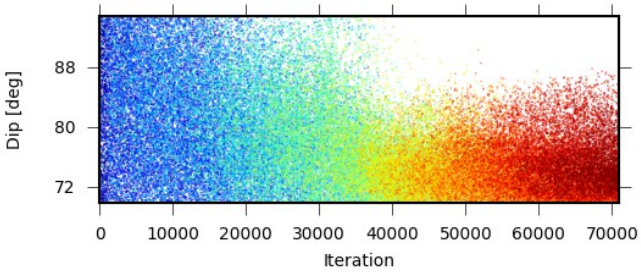
Dip [deg]
88
80
72
0
10000
20000
30000
40000
50000
60000
70000
Iteration

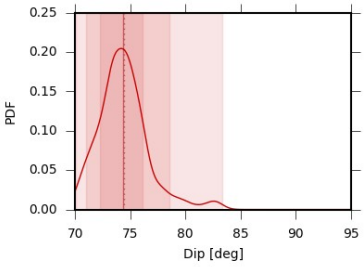
PDF
0.25
0.20
0.15
0.10
0.05
0.00
70
75
80
85
90
95
Dip [deg]

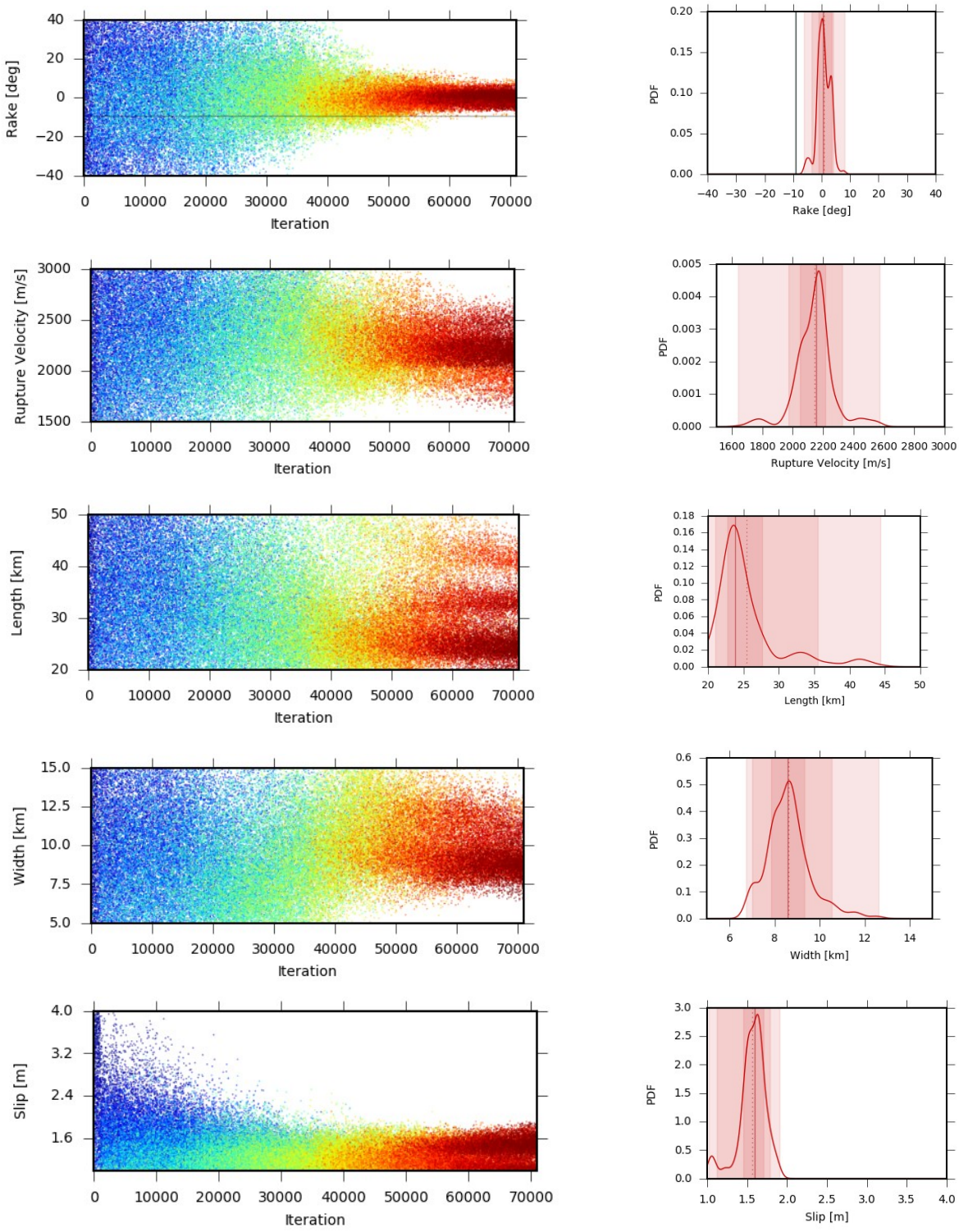

Figure S13. Left: Sequence plot, distribution and uncertainties of the some source parameters of the finite fault model (Slip, dip, rake, strike, width, length and rupture velocity). For details see caption of Fig. S8.

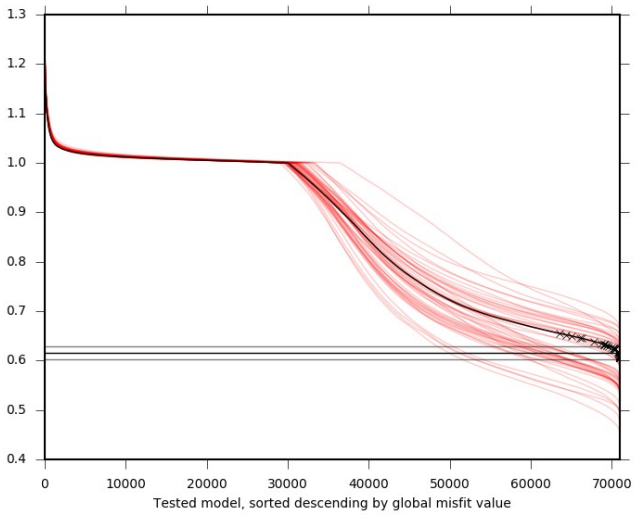

Figure S14. Bootstrap misfit of the optimization in 70000 iterations for the finite fault model. For details see caption of Fig. S9.

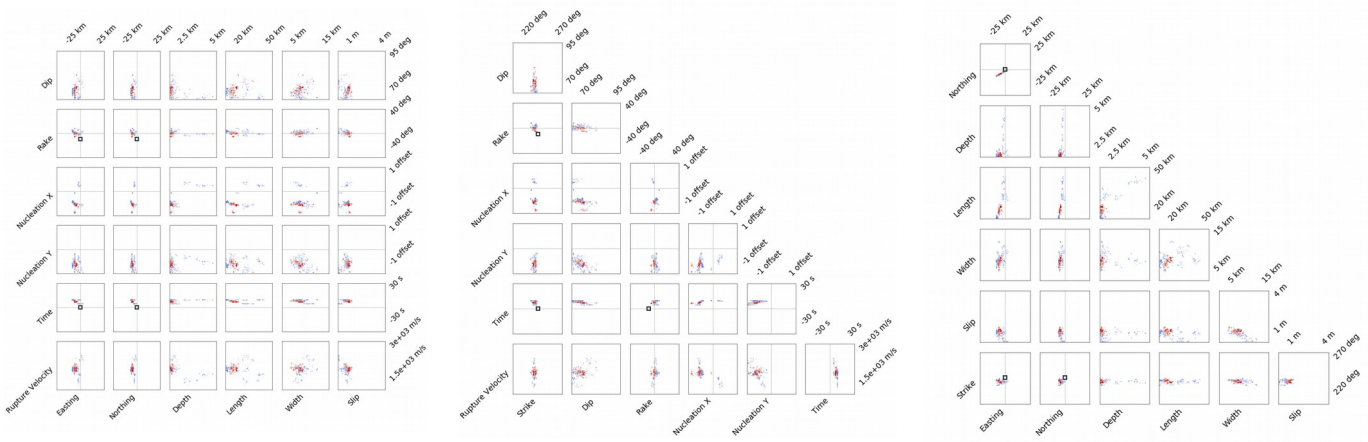

Figure S15. Source parameter's scatter plots, to evaluate the resolution of source parameters in finite fault model and trade-offs between pairs of model parameters. For details see caption of Fig. S11.

Moment tensor inversion results of the fore and after shocks:

Table S1. Our results of the focal mechanism solutions of fore and after shocks of the 24 January 2020 Elazığ-Sivrice earthquake with comparing to the other agencies. GEOFON: GFZ German Research Center for Geosciences. AFAD: Disaster and Emergency Management Authority Presidential of Earthquake Department. GCMT: Global Centroid Moment Tensor.

Date	Time (UTC)	Source	Latitude°	Longitude°	Strike1 °	Dip1 °	Rake1 °	Strike2 °	Dip2 °	Rake2 °	Depth (km)	Seismic Moment (N.M)	Mw
4 April 2009	17:31:07.00	AFAD	38.3865	39.1205	345	84	173	76	83	6	9.7	6.90E+016	5.2
		GEOFON	38.38	39.09	342	86	174	73	84	4	10		5.2
		GCMT	38.35	39.06	339	71	-173	246	83	-20	12	9.75E+016	5.3
		This study	38.3865	39.1205	67.53	82.49	23.76	334.24	66.44	171.8	3.66	6.41E+16	5.17
27 December 2019	07:02:25.00	AFAD	38.3898	39.0158	346	86	-139	252	50	-6	15.1	2.53E+016	4.9
		GEOFON	38.31	39.07	345	89	167	75	77	1	14		4.8
		This study	38.3898	39.0158	257.16	32.72	6.45	161.72	86.51	122.56	7.76	2.45E+16	4.89
25 January 2020	00:48:51.00	AFAD	38.4883	39.203	271	68	2	180	88	158	9.2	1.80E+013	4.3
		This study	38.4883	39.203	239.7	34.33	-61.3	26.16	60.34	-108.16	5.98	2.02E+15	4.17
25 January 2020	06:07:33.00	AFAD	38.3848	39.0368	336	80	-158	242	69	-10	8.2	2.15E+15	4.2
		This study	38.3848	39.0368	244.83	48.28	-7.97	340.15	84.05	-138	5.55	2.08E+15	4.17
25 January 2020	08:40:03.00	AFAD	38.479	39.2895	246	67	-9	339	81	-157	10.1	2.32E+013	4.5
		This study	38.479	39.2895	61.27	69.68	6.81	328.89	83.61	159.55	17.83	3.08E+15	4.29
25 January 2020	10:14:56.00	AFAD	38.276	38.753	245	81	-21	338	68	-169	11.5	2.16E+013	4.4
		This study	38.276	38.753	238.11	78.65	-65.18	351.15	27.13	-154.45	3.32	7.05E+15	4.53
25 January 2020	16:30:07.00	AFAD	38.374	39.131	244	58	-7	338	84	-148	12.4	3.03E+016	5
		GEOFON	38.36	39.2	327	80	167	59	78	11	10		5.1
		This study	38.374	39.131	58.61	77.24	18.02	324.5	72.43	166.6	6.72	3.31E+16	4.97
26 January 2020	02:22:45.00	AFAD	38.244	38.8013	324	89	176	54	86	1	7.2	2.87E+013	4.5
		This study	38.244	38.8013	233.54	78.04	-17.69	327.32	72.7	-167.47	3.7	5.64E+15	4.46
27 January 2020	16:12:00.00	AFAD	38.395	39.1333	165	84	-172	75	82	-6	11.94	2.69E+013	4.3
		This study	38.395	39.1333	248.13	82.61	-35.55	343.38	54.78	-170.94	2.95	3.80E+15	4.35
31 January 2020	23:32:49.00	AFAD	38.4916	39.3286	212	85	-14	303	76	-175	17.1	1.44E+016	4.6
		This study	38.4916	39.3286	304.09	72.7	-151.25	204.83	62.66	-19.55	10.21	9.17E+15	4.6
1 February 2020	00:03:49.00	AFAD	38.4511	39.2505	53	83	-10	144	80	-173	11.1	2.90E+013	4.3
		This study	38.4511	39.2505	58.72	77.07	-23.77	154.34	66.85	-165.92	4.29	2.11E+15	4.18
3 February 2020	22:19:40.00	AFAD	38.3986	39.1543	240	85	22	148	69	175	10.2	7.78E+014	4.6
		GEOFON	38.39	39.1	336	72	-177	246	88	-17	10		4.5
		This study	38.3986	39.1543	64.24	59.18	-6.99	157.83	83.99	-149	3.7	7.36E+15	4.54
17 February 2020	11:42:13.00	AFAD	38.396	39.115	155	89	-174	65	84	-1	9.1	3.92E+014	4.3
		This study	38.396	39.115	66.73	62.47	-5.61	159.33	85.02	-152.35	5.89	3.76E+15	4.35
25 February 2020	23:03:36.00	AFAD	38.3291	38.7696	245	43	-15	346	80	-132	9.1	3.19E+017	5
		GEOFON	38.27	38.84	230	39	-30	345	71	-124	10	2.90E+16	4.9
		This study	38.3291	38.7696	241.79	30.71	-14.49	344.33	82.65	-119.91	12.1	3.08E+16	4.95
27 February 2020	02:48:45.00	AFAD	38.2525	38.6566	346	59	-136	229	54	-40	12.1	2.97E+016	4.3
		This study	38.2525	38.6566	233.46	22.98	-27.28	348.86	79.68	-110.65	6.88	3.12E+015	4.29
29 February 2020	12:29:46.00	This study	38.4421	39.2356	239.88	76.34	-13.05	333.01	77.32	-165.99	3.94	5.14E+015	4.44
19 March 2020	17:53:31.00	AFAD	38.372	39.1041	75	82	-6	165	84°	172	7.3	3.01947E+017	5
		GEOFON	38.38	39.01	69	77	-4	160	85	-167	10		5.1
		This study	38.372	39.1041	66	70	4	335	86.4	160	5.58	4.06643E+016	5.04

Reference:

Basili, R., Kastelic, V., Demircioglu, M. B., Garcia Moreno D., et al.: The European Database of Seismogenic Faults (EDSF) compiled in the framework of the Project SHARE. http://diss.rm.ingv.it/share-edsf/, doi: 10.6092/INGV.IT-SHARE-EDSF, 2013.

Disaster and Emergency Management Authority Presidential of Earthquake Department (AFAD), https://deprem.afad.gov.tr, last access: 31 March 2020.

GEOFON Data Centre of Deutsches GeoForschungsZentrum GFZ. https://doi.org/10.14470/tr560404, Last access: 31 march 2020.

Global Centroid Moment Tensor (GCMT), https://www.globalcmt.org/, Last access: 31 march 2020.

Heimann, S., Isken, M., Kühn, D., Sudhaus, H., Steinberg, A., Vasyura-Bathke, H., Daout, S., Cesca, S., and Dahm, T.: Grond – A probabilistic earthquake source inversion framework, GFZ Data Services, https://doi.org/10.5880/GFZ.2.1.2018.003, 2018.